Inorganic Chemistry

Article

pubs.acs.org/IC

Visible and NIR Photoluminescence Properties of a Series of Novel Lanthanide–Organic Coordination Polymers Based on Hydroxyquinoline–Carboxylate Ligands

Yan-Li Gai,[†,‡] Ke-Cai Xiong,[†,‡] Lian Chen,[†] Yang Bu,[†,‡] Xing-Jun Li,[†,‡] Fei-Long Jiang,*[,†] and Mao-Chun Hong*[,†]

[†]State Key Laboratory of Structure Chemistry, Fujian Institute of Research on the Structure of Matter, Chinese Academy of Sciences, Fuzhou, 350002, China

[‡]Graduate School of the Chinese Academy of Sciences, Beijing, 100049, China

Supporting Information

ABSTRACT: A series of novel two-dimensional (2D) lanthanide coordination polymers with 4-hydroxyquinoline-2-carboxylate (H_2hqc) ligands, $[Ln(Hhqc)_3(H_2O)]_n \cdot 3nH_2O$ (Ln = Eu (**1**), Tb (**2**), Sm (**3**), Nd (**4**), and Gd (**5**)) and $[Ln(Hhqc)(ox)(H_2O)_2]_n$ (Ln = Eu (**6**), Tb (**7**), Sm (**8**), Tm (**9**), Dy (**10**), Nd (**11**), Yb (**12**), and Gd (**13**); H_2ox = oxalic acid), have been synthesized under hydrothermal conditions. Complexes **1**–**5** are isomorphous, which can be described as a two-dimensional (2D) hxl/Shubnikov network based on $Ln_2(CO_2)_4$ paddle-wheel units, and the isomorphous complexes **6**–**13** feature a 2D decker layer architecture constructed by Ln-ox infinite chains cross-linked alternatively by bridging $Hhqc^-$ ligands. The room-temperature photoluminescence spectra of complexes Eu^{III} (**1** and **6**), Tb^{III} (**2** and **7**), and Sm^{III} (**3** and **8**) exhibit strong characteristic emissions in the visible region, whereas Nd^{III} (**4** and **11**) and Yb^{III} (**12**) complexes display NIR luminescence upon irradiation at the ligand band. Moreover, the triplet state of H_2hqc matches well with the emission level of Eu^{III}, Tb^{III}, and Sm^{III} ions, which allows the preparation of new optical materials with enhanced luminescence properties.

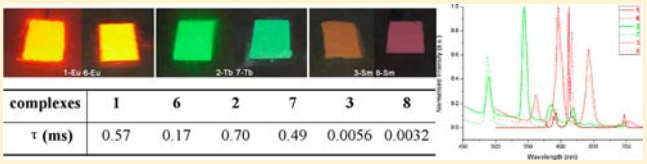

complexes	1	6	2	7	3	8
τ (ms)	0.57	0.17	0.70	0.49	0.0056	0.0032

INTRODUCTION

Luminescence from lanthanides has attracted extensive interest, because of their fascinating optical properties and a host of applications, such as biomedical analysis, medical diagnosis, cell imaging, and light-emitting diodes.[1] In fact, the chemistry and spectroscopy of these ions differ considerably from d-shell transition-metal ions in that the shielding of the 4f orbitals by the filled $5p^6 6s^2$ subshells results in special optical features of lanthanide ions with characteristic narrow line-like emissions of optical pure colors that are nearly unaffected by the ligand field.[2] All the lanthanide ions, except La^{III} and Lu^{III}, are luminescent, with emission spanning over the entire spectrum from ultraviolet (UV) (Gd^{III}) to visible (Sm^{III}, Eu^{III}, Tb^{III}, Dy^{III}, and Tm^{III}) and near-infrared (NIR) (Nd^{III}, Yb^{III}, and Er^{III}) regions. Gaining greater understanding of the luminescent lanthanides, it is found that Eu^{III} and Tb^{III} complexes are used extensively as optical materials or analytical sensors for their strong, visible, and easily detected emissions,[3] while NIR-emitting lanthanide ions Nd^{III}, Yb^{III}, and Er^{III} are ever-growing studied in biological analysis, because of their almost-transparent emissions in biological issues, which can improve the signal-to-noise (S/N) ratio significantly.[4]

Despite the optical purity and easily recognized emissions of lanthanide ions, the spin- and parity-forbidden nature of the f–f transitions renders direct photoexcitation of lanthanide ions disfavored, which makes their absorption coefficients usually smaller than 10 M^{-1} cm^{-1}. Therefore, the introduction of organic ligands function as chromophores to absorb light and transfer this energy to the excited states of the central lanthanide ions, which is the so-called "antenna effect", plays a notable role in the improvement of emission efficiency.[5] As a consequence, a number of chromophoric antenna ligands, especially the β-diketonate[6] and carboxylate ligands,[7] which have received the most attention, have been developed in an effort to achieve brighter lanthanide luminescence. Since tris-8-(hydroxyquinoline) aluminum was reported as an efficient electroluminescence material in the middle of the 1980s,[8] several hydroxyquinoline ligands have been attracting considerable attention as a chromophoric antenna for constructing lanthanide coordination polymers. However, there is a major disadvantage to obtain the crystalline products for structure determination, because of the insolubility of the parent lanthanoid-hydroxyquinolines.[9] In this study, enhancement of solubility can be achieved by introducing carboxyl substitution into hydroxyquinoline ligand, and thereby facilitate syntheses and crystallizations of complex molecules. In addition, the introduction of the carboxyl groups with sufficiently strong binding capacity would preclude the coordination of water molecules to metal centers in the first coordination sphere,

Received: June 13, 2012
Published: December 3, 2012

   dx.doi.org/10.1021/ic301261g | Inorg. Chem. 2012, 51, 13128–13137

Table 1. Crystallographic Data for Complexes 1−13

	1	2	3	4	5	6	7
empirical formula	$C_{30}H_{26}EuN_3O_{13}$	$C_{30}H_{26}TbN_3O_{13}$	$C_{30}H_{26}SmN_3O_{13}$	$C_{30}H_{26}NdN_3O_{13}$	$C_{30}H_{26}GdN_3O_{13}$	$C_{12}H_{10}EuNO_9$	$C_{12}H_{10}TbNO_9$
formula weight	788.50	795.46	786.89	780.78	793.79	464.17	471.13
crystal system	monoclinic	monoclinic	monoclinic	monoclinic	monoclinic	monoclinic	monoclinic
space group	$P2_1/c$	$P2_1/c$	$P2_1/c$	$P2_1/c$	$P2_1/c$	$P2_1/c$	$P2_1/c$
a (Å)	12.1224(18)	12.131(2)	12.139(3)	12.1434(18)	12.129(3)	7.9229(10)	7.9196(6)
b (Å)	25.352(4)	25.337(5)	25.449(6)	25.812(7)	25.379(6)	11.8032(16)	11.7236(7)
c (Å)	9.7713(14)	9.8149(18)	9.828(2)	9.940(3)	9.818(2)	15.062(3)	15.0130(10)
α (°)	90	90	90	90	90	90	90
β (°)	92.862(3)	92.879(4)	92.826(5)	93.054(14)	92.835(4)	104.899(8)	105.072(4)
γ (°)	90	90	90	90	90	90	90
V (Å^3)	2999.2(8)	3013.1(10)	3032.4(12)	3111.2(13)	3018.5(12)	1361.2(4)	1345.95(16)
Z	4	4	4	4	4	4	4
D_c (g cm^{-3})	1.746	1.754	1.724	1.667	1.747	2.265	2.325
μ (mm^{-1})	2.166	2.422	2.011	1.741	2.272	4.659	5.307
F (000)	1576	1584	1572	1564	1580	896	904
θ range (°)	2.63−27.48	3.36−27.47	2.62−27.48	2.20−27.44	2.32−27.47	3.17−25.00	2.81−27.48
reflections measured	26071	26644	23293	23795	22864	8353	10177
independent reflections	6809	6665	6923	7032	6895	2344	2996
goodness-of-fit on F^2	1.031	1.100	1.025	1.130	1.159	1.047	1.038
R_{int}	0.0300	0.0427	0.0214	0.0727	0.0188	0.0141	0.0180
R_1 ($I > 2\sigma(I)$)[a]	0.0205	0.0339	0.0257	0.0564	0.0231	0.0134	0.0166
wR_2 ($I > 2\sigma(I)$)[b]	0.0486	0.0638	0.0581	0.1141	0.0591	0.0340	0.0395

	8	9	10	11	12	13
empirical formula	$C_{12}H_{10}SmNO_9$	$C_{12}H_{10}TmNO_9$	$C_{12}H_{10}DyNO_9$	$C_{12}H_{10}NdNO_9$	$C_{12}H_{10}YbNO_9$	$C_{12}H_{10}GdNO_9$
formula weight	462.56	481.14	474.71	456.45	485.25	469.46
crystal system	monoclinic	monoclinic	monoclinic	monoclinic	monoclinic	monoclinic
space group	$P2_1/c$	$P2_1/c$	$P2_1/c$	$P2_1/c$	$P2_1/c$	$P2_1/c$
a (Å)	7.9055(12)	7.930(2)	7.9262(7)	7.9003(14)	7.936(3)	7.8436(16)
b (Å)	11.8535(17)	11.564(3)	11.6805(8)	11.960(2)	11.523(4)	11.760(2)
c (Å)	15.099(3)	14.913(4)	14.9892(12)	15.170(3)	14.890(5)	14.978(3)
α (°)	90	90	90	90	90	90
β (°)	104.729(3)	105.548(11)	105.178(5)	104.444(3)	105.696(17)	104.322(5)
γ (°)	90	90	90	90	90	90
V (Å^3)	1368.4(4)	1317.5(6)	1339.32(18)	1388.1(4)	1310.9(8)	1338.7(5)
Z	4	4	4	4	4	4
D_c (g cm^{-3})	2.245	2.426	2.354	2.184	2.459	2.329
μ (mm^{-1})	4.343	6.787	5.632	3.791	7.188	5.007
F (000)	892	920	908	884	924	900
θ range (°)	3.73−27.49	2.26−27.48	2.66−27.47	2.77−27.47	2.84−27.48	3.19−27.45
reflections measured	9753	13710	14368	12922	9325	9585
independent reflections	3121	3017	3065	3160	2986	2976
goodness-of-fit on F^2	1.048	1.073	1.076	1.063	1.003	1.103
R_{int}	0.0186	0.0443	0.0379	0.0177	0.0200	0.0213
R_1 ($I > 2\sigma(I)$)[a]	0.0166	0.0202	0.0195	0.0163	0.0162	0.0159
wR_2 ($I > 2\sigma(I)$)[b]	0.0410	0.0471	0.0477	0.0379	0.0382	0.0417

[a] $R_1 = \sum||F_o| - |F_c||/\sum|F_o|$. [b] $wR_2 = [\sum w(F_o^2 - F_c^2)^2/\sum w(F_o^2)^2]^{1/2}$.

therefore reducing the activation of nonradiative decay processes. Furthermore, hydroxyquinoline carboxylate ligands also draw attention to their inherent chemical features: (a) carboxyl group can readily coordinate to lanthanide ions because of the strong affinity between oxygen atoms and lanthanide ions; (b) the $\pi \rightarrow \pi^*$ transitions of the organic ligands cause strong absorption in the UV region, which is efficient to sensitize lanthanide emissions through energy transfer in terms of ligand (S1) → ligand (T1) → Ln*; (c) the robustness and a certain degree of rigidity to the framework provided by the aromaticity in the organic backbone hinder the nonradiative deactivation process.

Given the important potential applications of lanthanide coordination polymers and the fascinating properties of hydroxyquinoline carboxylate ligands, we have been intrigued to prepare a series of lanthanide complexes based on lanthanide chlorides, 4-hydroxyquinoline-2-carboxylate (H_2hqc) and oxalic acid (H_2ox), which are rarely reported coordination polymers of such types of ligands.[10] All structures of the newly synthesized complexes have been elucidated by single-crystal X-ray diffraction, powder X-ray diffractometry (PXRD), infrared (IR) spectroscopy, thermogravimetric analysis (TGA), and elemental analysis. The optical properties of all complexes have been investigated as well as the mechanism of

dx.doi.org/10.1021/ic301261g | Inorg. Chem. 2012, 51, 13128−13137

energy transfer correlated with the singlet and triplet energy levels of the ligands has been determined from the room-temperature UV−vis absorption spectra and the 77 K emission spectra of the corresponding Gd^{III} complex.

EXPERIMENTAL SECTION

Materials and Methods. All reagents and solvents were purchased commercially and used without further purification. Elemental analyses (C, H, and N) were performed on a Vario EL III elemental analyzer. IR spectra were recorded in the range of 4000−400 cm^{-1} with a Magna 750 FT-IR spectrometer using KBr pellets. TGA analyses were carried out in the temperature range of 30−900 °C, with a heating rate of 15 °C/min on a Netzsch Model STA 449C instrument. PXRD patterns were collected on a Rigaku Model DMAX 2500 diffractometer with Cu Kα radiation (λ = 1.5406 Å). The UV−vis absorption spectra were collected on a Lambda-900 instrument from the Perkin−Elmer Corporation. Emission and excitation spectra were recorded on a Horiba Jobin−Yvon Fluorolog-3 spectrophotometer analyzer. Time-resolved fluorescence were performed on an Edinburgh Instruments Model FLS920 spectrofluorometer equipped with both a continuous (450-W) xenon lamp and a pulse xenon lamp.

Syntheses of Complexes 1−5. A mixture of $LnCl_3{\cdot}6H_2O$ (0.3 mmol) (Ln = Eu, Tb, Sm, Nd, and Gd), H_2hqc (0.2 mmol), NaOH (0.2 mmol), and H_2O (10 mL) was sealed in a 25-mL Teflon-lined stainless steel autoclave under autogenous pressure at 160 °C for 4 days. After slowly cooling to room temperature at a rate of 5 °C/h, the yellow prism-shaped crystals suitable for X-ray structural analysis were obtained by filtration, washed with ethanol, and dried in air.

$[Eu(Hhqc)_3(H_2O)]_n{\cdot}3nH_2O$ ***(1)***. Elemental analysis (%): Calcd for $C_{30}H_{26}Eu_1N_3O_{13}$: C, 45.69; H, 3.37; N, 5.33. Found: C, 45.44; H, 3.37; N, 5.32. IR (KBr, cm^{-1}): 3428(m), 3068(w), 1630(s), 1599(s), 1542(m), 1515(m), 1474(m), 874(w), 776(w), 669(w).

$[Tb(Hhqc)_3(H_2O)]_n{\cdot}3nH_2O$ ***(2)***. Elemental analysis (%): Calcd for $C_{30}H_{26}Tb_1N_3O_{13}$: C, 45.29; H, 3.29; N, 5.28. Found: C, 45.06; H, 3.34; N, 5.28. IR (KBr, cm^{-1}): 3408(m), 3067(w), 1684(s), 1598(s), 1516(m), 1474(m), 1432(m), 867(w), 776(w), 669(w).

$[Sm(Hhqc)_3(H_2O)]_n{\cdot}3nH_2O$ ***(3)***. Elemental analysis (%): Calcd for $C_{30}H_{26}Sm_1N_3O_{13}$: C, 45.79; H, 3.33; N, 5.34. Found: C, 45.80; H, 3.38; N, 5.34. IR (KBr, cm^{-1}): 3399(m), 3067(w), 1626(s), 1598(s), 1515(m), 1474(m), 1443(m), 874(w), 775(w), 668(w).

$[Nd(Hhqc)_3(H_2O)]_n{\cdot}3nH_2O$ ***(4)***. Elemental analysis (%): Calcd for $C_{30}H_{26}Nd_1N_3O_{13}$: C, 46.15; H, 3.36; N, 5.38. Found: C, 46.05; H, 3.39; N, 5.36. IR (KBr, cm^{-1}): 3406(m), 3068(w), 1626(s), 1598(s), 1513(m), 1474(m), 1443(m), 874(w), 775(w), 669(w).

$[Gd(Hhqc)_3(H_2O)]_n{\cdot}3nH_2O$ ***(5)***. Elemental analysis (%): Calcd for $C_{30}H_{26}Gd_1N_3O_{13}$: C, 45.39; H, 3.30; N, 5.29. Found: C, 45.46; H, 3.28; N, 5.35. IR (KBr, cm^{-1}): 3411(m), 3069(w), 1627(s), 1542(s), 1516(m), 1474 (m), 1434(m), 874(w), 776(w), 669(w).

Syntheses of Complexes 6−13. A mixture of $LnCl_3{\cdot}6H_2O$ (0.3 mmol) (Ln = Eu, Tb, Sm, Tm, Dy, Nd, Yb, and Gd), H_2hqc (0.2 mmol), oxalic acid (0.2 mmol), and H_2O (10 mL) was sealed in a 25-mL Teflon-lined stainless steel autoclave under autogenous pressure at 160 °C for 4 days. After slowly cooling to room temperature at 5 °C/h, the light yellow rhombic-shaped single crystals were obtained by filtration, washed with ethanol, and dried in air.

$[Eu(Hhqc)(ox)(H_2O)_2]_n$ ***(6)***. Elemental analysis (%): Calcd for $C_{12}H_{10}Eu_1N_1O_9$: C, 31.05; H, 2.17; N, 3.02. Found: C, 31.12; H, 2.22; N, 2.98. IR (KBr, cm^{-1}): 3603(m), 3151(s), 1626(s), 1594(s), 1505(m), 1471(m), 1407(m), 867(w), 792(w), 741(w).

$[Tb(Hhqc)(ox)(H_2O)_2]_n$ ***(7)***. Elemental analysis (%): Calcd for $C_{12}H_{10}Tb_1N_1O_9$: C, 30.59; H, 2.14; N, 2.97. Found: C, 30.45; H, 2.24; N, 2.92. IR (KBr, cm^{-1}): 3604(m), 3149(s), 1627(s), 1594(s), 1507(m), 1472(m), 1407(m), 867(w), 796(w), 742(w).

$[Sm(Hhqc)(ox)(H_2O)_2]_n$ ***(8)***. Elemental analysis (%): Calcd for $C_{12}H_{10}Sm_1N_1O_9$: C, 31.16; H, 2.18; N, 3.02. Found: C, 31.18; H, 2.25; N, 2.99. IR (KBr, cm^{-1}): 3602(m), 3152(s), 1625(s), 1594(s), 1505(m), 1471(m), 1407(m), 867(w), 791(w), 741 (w).

$[Tm(Hhqc)(ox)(H_2O)_2]_n$ ***(9)***. Elemental analysis (%): Calcd for $C_{12}H_{10}Tm_1N_1O_9$: C, 29.96; H, 2.09; N, 2.91. Found: C, 30.11; H, 2.13; N, 2.84. IR (KBr, cm^{-1}): 3607(m), 3142(s), 1631(s), 1594(s), 1508(m), 1473(m), 1408(m), 866(w), 795(w), 743(w).

$[Dy(Hhqc)(ox)(H_2O)_2]_n$ ***(10)***. Elemental analysis (%): Calcd for $C_{12}H_{10}Dy_1N_1O_9$: C, 30.36; H, 2.12; N, 2.95. Found: C, 30.54; H, 2.07; N, 2.92. IR (KBr, cm^{-1}): 3605(m), 3148(s), 1629(s), 1594(s), 1508(m), 1473(m), 1408(m), 866(w), 794(w), 743(w).

$[Nd(Hhqc)(ox)(H_2O)_2]_n$ ***(11)***. Elemental analysis (%): Calcd for $C_{12}H_{10}Nd_1N_1O_9$: C, 31.58; H, 2.21; N, 3.07. Found: C, 31.57; H, 2.14; N, 3.11. IR (KBr, cm^{-1}): 3601(m), 3153(s), 1625(s), 1594(s), 1504(m), 1471(m), 1406(m), 868(w), 789(w), 739(w).

$[Yb(Hhqc)(ox)(H_2O)_2]_n$ ***(12)***. Elemental analysis (%): Calcd for $C_{12}H_{10}Yb_1N_1O_9$: C, 29.70; H, 2.08; N, 2.89. Found: C, 29.54; H, 2.14; N, 2.79. IR (KBr, cm^{-1}): 3608(m), 3137(s), 1636(s), 1594(s), 1509(m), 1472(m), 1408(m), 866(w), 796(w), 744(w).

$[Gd(Hhqc)(ox)(H_2O)_2]_n$ ***(13)***. Elemental analysis (%): Calcd for $C_{12}H_{10}Gd_1N_1O_9$: C, 30.70; H, 2.15; N, 2.98. Found: C, 30.45; H, 2.21; N, 2.96. IR (KBr, cm^{-1}): 3604(m), 3151(s), 1626(s), 1594(s), 1507(m), 1471(m), 1407(m), 867(w), 793(w), 741(w).

X-ray Crystallographic Determination. The X-ray diffraction data of complexes **1** and **13** were collected on a Rigaku Saturn 724+ CCD diffractometer with a confocal−monochromatic Mo Kα radiation source (λ = 0.71073 Å) at 123 K. While complex **2** was determined on a Rigaku Saturn 70 CCD diffractometer at 293 K, complexes **3**−**12** were determined on a Rigaku Mercury CCD diffractometer at 293 K, which were both equipped with graphite-monochromatic Mo Kα radiation. All of the structures were resolved by the direct method and refined by full-matrix least-squares fitting on F^2 by SHELX-97.[11] All non-hydrogen atoms, except some of the solvent molecules, were refined with anisotropic thermal parameters. The positions of hydrogen atoms on the organic ligands were generated geometrically and refined using a riding model. The hydrogen atoms on water molecules were located in different density maps and were refined as riding, using the instruction AFIX 3, while the hydrogen atoms of water molecules that cannot be generated were included in the molecular formula directly. CCDC-878315−878327 (**1**−**13**) contain the supplementary crystallographic data for this paper. These data can be obtained free of charge from the Cambridge Crystallographic Data Center via www.ccdc.cam.ac.uk/data_request/cif. The summary of crystallographic data and structure refinements for **1**−**13** is listed in Table 1. The selected bond lengths and angles of complexes **1**−**13** are listed in Table S1 in the Supporting Information, respectively.

DISCUSSION

Syntheses and Structures. All the complexes were synthesized by hydrothermal reactions at 160 °C, with the addition of different Lewis acids and bases to adjust the pH value. Complexes **1**−**5** were obtained in the presence of NaOH with the pH value of ∼5, while complexes **6**−**13** were generated under the employment of H_2ox, which acted as an ancillary ligand binding to lanthanide ions. With regard to the syntheses, complexes **1**−**5** can be obtained under the variation of pH values from 1 to 14 in the presence of HCl or NaOH. Therefore, it suggests that the pH value has just a minuscule effect on the formation and crystalline morphology of the above products.

Single-crystal X-ray diffraction (XRD) analyses reveal that complexes **1**−**5** and **6**−**13** are isomorphous, respectively. All complexes assemble to three-dimensional (3D) supramolecular structures through hydrogen bonding or $\pi\cdots\pi$ interactions based on two-dimensional (2D) sheet architectures. The average bond lengths of Ln−O decrease sequentially from Nd to Yb for **1**−**13** with increasing atomic number, because of the lanthanide contraction effect.[12] The structural evidence demonstrates that the H_2hqc ligand is capable of binding trivalent lanthanide ions with hard Lewis base oxygen atoms of carboxyl and hydroxyl groups.

dx.doi.org/10.1021/ic301261g | Inorg. Chem. 2012, 51, 13128−13137

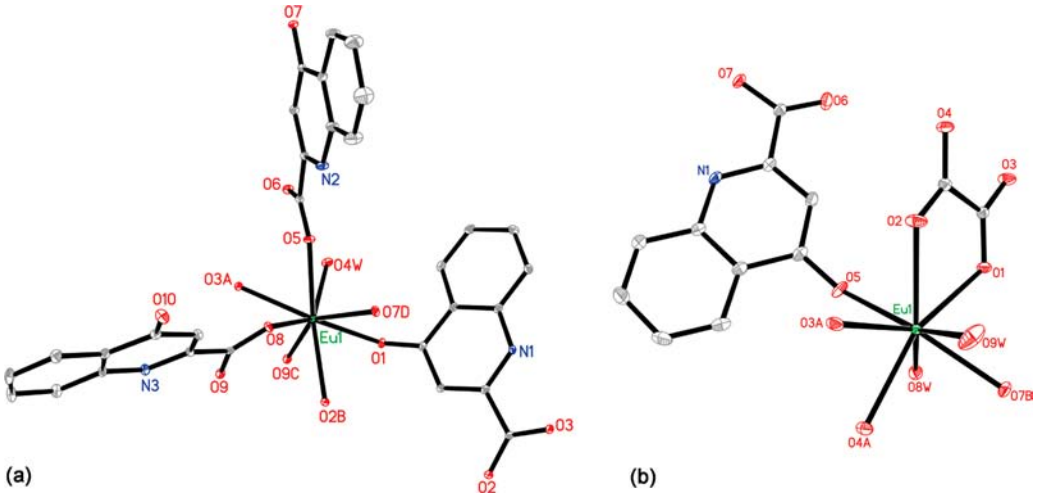

Figure 1. Coordination environment of the Eu^{III} ion (a) in **1** with 30% thermal ellipsoids and (b) in **6** with 30% thermal ellipsoids. (All hydrogen atoms and solvent molecules are omitted for clarity.)

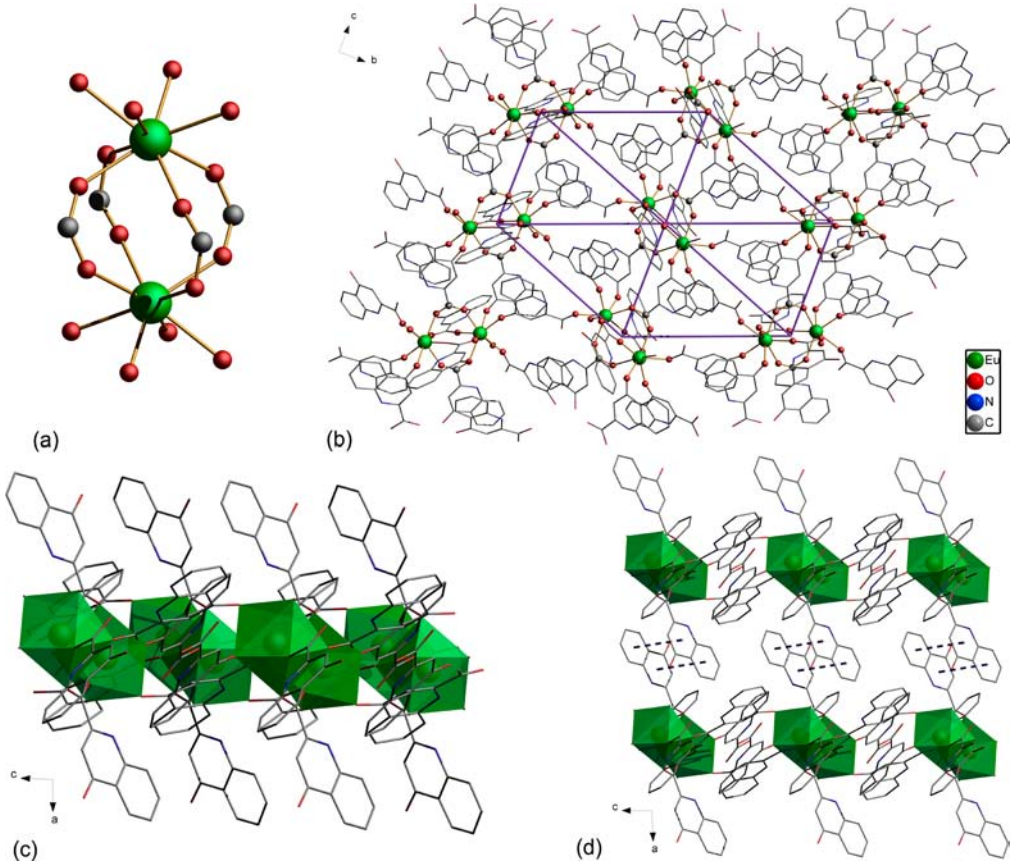

Figure 2. (a) Structure of a paddle-wheel unit for **1**. (b) 2D layer of **1** running along the *bc*-plane. (c) The 2D layer of **1** propagating along the *ac*-plane. (d) The 3D framework of **1** connected by $\pi\cdots\pi$ interactions (denoted by the dotted lines) along the *b*-axis.

Crystal Structures of $[Ln(Hhqc)_3(H_2O)]_n\cdot 3nH_2O$ (Ln = Eu (1), Tb (2), Sm (3), Nd (4), Gd (5)). X-ray crystallography reveals that complexes **1**−**5** are isomorphous, so complex **1** is employed as a representative to be discussed in detail. Complex **1**, crystallizing in the monoclinic system and space group $P2_1/c$, features a 2D network based on $Eu_2(CO_2)_4$ paddle-wheel units. As shown in Figure 1a, the asymmetric unit of **1** consists of one crystallographically independent Eu^{III} ion, three $Hhqc^-$ ligands, one coordinated water molecule and three lattice water molecules. Each Eu^{III} is surrounded by an O_8 donor set, formed by five carboxylate oxygen atoms, two hydroxyl oxygen atoms, and one terminal water molecule. The coordination geometry around the metal center can be described as a distorted square antiprism. The Eu−O bond lengths vary from 2.293(1) Å to 2.464(1) Å, which correspond to those reported for other lanthanide−oxygen donor complexes.[13] Eu1 and its corresponding centrosymmetric generated atom Eu1A are joined by four μ_2-O atoms of carboxylate groups to form a binuclear paddle-wheel unit, with the separation of Eu···Eu being 4.392 Å (Figure 2a). Each $Eu_2(CO_2)_4$ unit is connected

dx.doi.org/10.1021/ic301261g | *Inorg. Chem.* 2012, 51, 13128−13137

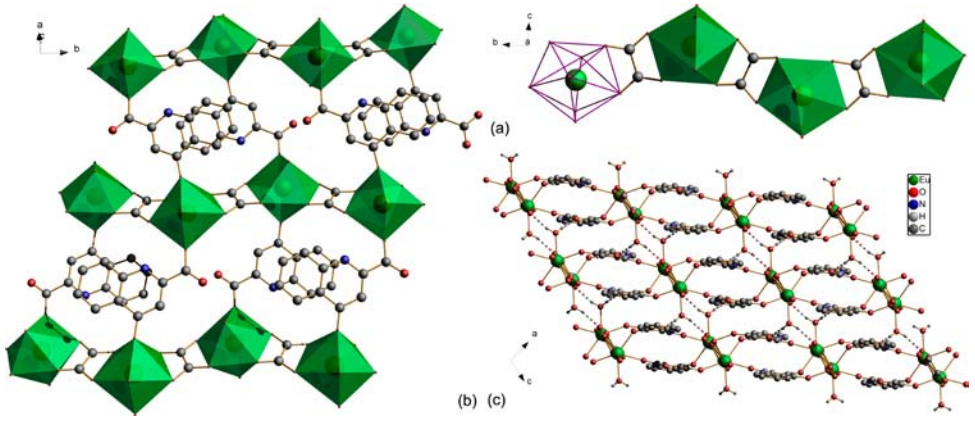

Figure 3. (a) 1D Eu-ox chain of **6** along the *b*-axis. (b) 2D layer of **6** propagating along the *ab*-plane. (c) 3D framework of **6** connected by O−H···O interaction in the *ac*-plane.

with six adjacent units through six $Hhqc^-$ ligands sustaining a 2D hxl/Shubnikov sheet along the *bc* plane, as illustrated in Figure 2b. The $Hhqc^-$ ligands connect the units through dimonodentate and trimonodentate bonding modes. However, there are a set of $Hhqc^-$ ligands that coordinate to the metal centers with terminal bridging-monodentate binding mode, which play a vital role in the extension of the dimensionality for **1**. As shown in Figures 2c and 2d, the quinoline rings of $Hhqc^-$ ligands are almost parallel within nearby layers, thus $\pi\cdots\pi$ interactions in face-to-face and partial overlapping take place, with the intercentroid distances being 3.567−3.968 Å. This weak interaction imparts the 2D monolayers extended to a 3D architecture. The crystallization O11w, O12w, and O13w water molecules are placed in the intermellar region, establishing strong hydrogen bonding interactions with the layer network. The topological analysis indicates a uninodal 2D hxl/Shubnikov (3,6) lane net with the point symbol being {3^6.4^6.5^3} when considering the binuclear paddle-wheel unit as a 6-connected node.

Crystal Structures of $[Ln(Hhqc)(ox)(H_2O)_2]_n$ (Ln = Eu (6), Tb (7), Sm (8), Tm (9), Dy (10), Nd (11), Yb (12), and Gd(13)). X-ray crystallography reveals that complexes **6**−**13** are isomorphous, crystallizing in the monoclinic system with the $P2_1/c$ space group, which can be described as 2D stacked $[Ln(Hhqc)(ox)(H_2O)_2]$ layers. Herein, complex **6** is represented to depict the detailed structure. As shown in Figure 1b, the asymmetric unit of **6** contains one crystallographically independent Eu^{III} ion, one $Hhqc^-$ ligand, one ox^{2-} ligand, and two coordinated water molecules. The metal center is eight-coordinated in an O_8 donor set, leading to a polyhedral geometry close to a triangular dodecahedron by four oxygen atoms from two ox^{2-}, one hydroxyl oxygen, and one carboxylate oxygen atoms from two different $Hhqc^-$ ligands, and two oxygen atoms from the coordinated water molecules. This type of configuration of eight-coordinated Eu^{III} ion is rarely reported, compared to the square antiprism, which is confirmed by comparing chosen ideal and observed pertinent dihedral angles based on calculations of the shape factor *S* to evaluate the degree of distortion from an ideal geometry.[14] The estimated *S* values of Eu^{III} ions are summarized in Tables S2 and S3 in the Supporting Information. The coordination Eu−O bond lengths, varying from 2.289(2) Å to 2.471(2) Å, are within the range observed for analogous reported.[15] As shown in Figure 3a, the adjacent metal centers are joined by ox^{2-}, generating corrugated Eu-ox chain that propagates along the crystallographic *b*-axis, with Eu···Eu separation of 6.289 Å. Each chain is linked parallel to its adjacent ones by means of the $Hhqc^-$ ligands, leading to a 2D decker sheet lying in the *ac*-plane, as illustrated in Figure 3b. The Eu···Eu distance across the bridging $Hhqc^-$ ligand is 10.031 Å. The $Hhqc^-$ ligand in **6** adopts a bridging monodentate binding mode, with the ox^{2-} ligands simply acting as a linker between two metal centers. The alternative bridging $Hhqc^-$ ligands that are almost parallel in monolayer connect to each other through partially overlapping $\pi\cdots\pi$ interactions with the shortest centroid−centroid distance being 3.735 Å, which provides certain rigidity to the 2D architecture. The sheets are piled up along the *b*-axis, creating an extended 3D architecture by means of hydrogen bonding interactions involving O8−H8A···O6c and O8−H8A···O4a between the coordinated water molecules and the carboxylate oxygen atoms in each sheet (Figure 3c). The O−H···O distances are 2.715(2) and 2.837(2) Å, and the O−H···O angles are 175.1° and 164.8°, respectively (symmetry codes: *a*, $x, {}^1/_2-y, z-{}^1/_2$; *c*, $3-x, {}^1/_2+y, {}^1/_2-z$).

THERMAL STABILITY AND POWDER X-RAY DIFFRACTION

The thermogravimetric analyses (TGA) were carried out on crystalline samples of **1**−**13** in the temperature range of 30−900 °C under a N_2 atmosphere. TGA curves of isomorphous complexes **1**−**5** and **6**−**13** are, respectively, similar, exhibiting one main weight loss step until the decomposition of the framework. Here, complexes **1** and **6** are used as two representatives as illustrated in Figure 4, and the thermogravimetric analyses of other complexes are provided as Figure S1 in the Supporting Information. The TGA trace for complex **1** displays a 5.62% weight loss between room temperature and 90 °C, which is consistent with the departure of three lattice water molecules (theoretical 5.71%). The remaining framework is thermally stable up to 340 °C, until which gradual collapse of the framework occurs. Complex **6** is stable up to 200 °C and exhibits one main step of weight loss. This mass loss (observed 7.76%, theoretical 7.76%) from 200 °C to 280 °C can be attributed to the release of two coordinated water molecules per formula unit. The remaining framework of **6** is stable within a temperature range of 280−400 °C. Upon further heating, the host framework begins to decompose.

The purity of the bulky crystalline samples was confirmed by PXRD. The PXRD patterns of complexes **1**−**13** are illustrated in Figure S2 in the Supporting Information, which are in good

dx.doi.org/10.1021/ic301261g | *Inorg. Chem.* 2012, 51, 13128−13137

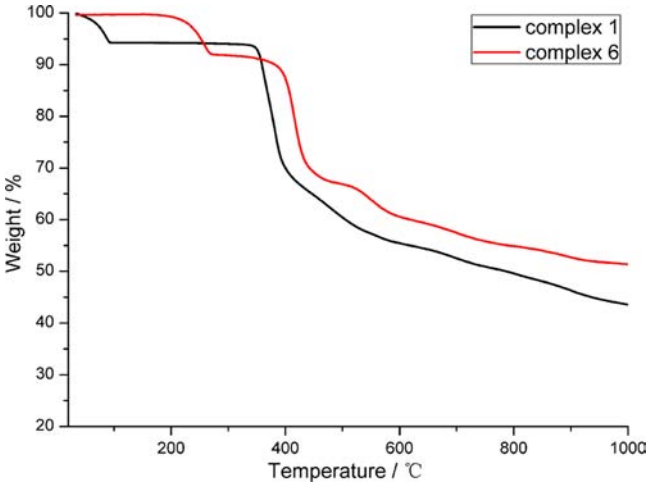

Figure 4. TGA diagrams of complexes **1** and **6**.

agreement with simulated ones, confirming the phase purity of the as-synthesized products.

UV–VIS ABSORPTION SPECTRA

The UV–vis absorption spectra of the free ligand and those corresponding Ln^{III} complexes recorded in dimethylformamide (DMF) solution (2×10^{-5} M) are displayed in Figure 5. The ligand H_2hqc displays two broad bands at 330 and 344 nm in the UV region, attributing to singlet–singlet $n \rightarrow \pi^*$ and $\pi \rightarrow \pi^*$ transitions. The absorption profile of each complex is identical to that observed for the free ligand in the range of 250–400 nm, indicating that the coordination of Ln^{III} ions does not significantly influence the energy of the singlet states of the H_2hqc ligand.

VISIBLE LUMINESCENT PROPERTIES OF EU-, TB-, AND SM-CENTERED COMPLEXES

The excitation and emission spectra of complexes **1** and **6** in the solid state at room temperature are shown in Figure 6a. The excitation spectra of both complexes are recorded by monitoring the strongest 614 nm emission band of Eu^{III} ion. They all show a broad band between 250 and 400 nm, which can be assigned to the $n \rightarrow \pi^*$ and $\pi \rightarrow \pi^*$ transitions of the coordinated ligand. Meanwhile, two sharp lines at 394 and 464 nm, which are characteristic of the Eu^{III} ion energy level, are also observed in the excitation spectra of both complexes, which are attributed to the transitions from the $^5L_6$ and $^5D_2$ to $^7F_{0,1}$. The emission spectra of both complexes excited at 360 nm show a similar pattern in the visible region, with sharp characteristic peaks at 578, 591, 614, 649, and 698 nm corresponding to the $^5D_0 \rightarrow {}^7F_J$ (J = 0–4) transitions, respectively. No broad emission band resulting from the ligand is observed, which demonstrates that the ligand transfers the absorbed energy effectively to the emitting level of the Eu^{III} center. The presence of the weak symmetry-forbidden $^5D_0 \rightarrow {}^7F_0$ emission, which is only allowed for C_s, C_n, and C_{nv} site symmetry according to the ED selection rule,[16] indicates that the Eu^{III} ions occupy low-symmetry coordination site with no inversion center, in agreement with the result of X-ray crystal structure analyses. The intensity of the $^5D_0 \rightarrow {}^7F_2$ transition (electric dipole), which is hypersensitive to the site symmetry of the Eu^{III} ion, is greater than that of the $^5D_0 \rightarrow {}^7F_1$ transition (magnetic dipole) indicating that the coordination environment of the Eu^{III} ions in **1** and **6** is devoid of an inversion center.[17]

Figure 6b presents the room-temperature excitation and emission spectra of complexes **2** and **7** in the solid state. Both excitation spectra, monitored around the more-intense 544-nm emission band of the Tb^{III} ion, exhibit a band in the 250–400 nm region associated with the $n \rightarrow \pi^*$ and $\pi \rightarrow \pi^*$ electronic transitions of the coordinated ligand. The absence of any absorption bands due to the f–f transition of Tb^{III} ion proves that the luminescence sensitization via excitation of the ligand is effective. The room-temperature emission spectra of **2** and **7** excited at 360 nm exhibit a series of sharp lines of the Tb^{III} ion, which result from the deactivation of the $^5D_4$ excited state to the corresponding ^7F_J ground state (J = 6, 5, 4, and 3) centered at 488, 544, 585, and 620 nm.

When H_2hqc ligand is introduced to sensitize the Sm^{III} ion, the emission spectra of **3** and **8** exhibit the typical emission bands of the Sm^{III} ion, upon excitation via the ligand-centered $n \rightarrow \pi^*$ and $\pi \rightarrow \pi^*$ transitions (360 nm), centered at 560, 595, 643, and 702 nm (Figure 6c), which are assigned to the transitions of $^4G_{5/2}$ to ^6H_J ($J = {}^5/_2, {}^7/_2, {}^9/_2$, and $^{11}/_2$). The weak ligand fluorescence appears in the emission spectra at 400–450 nm, signifying that the intramolecular energy transfer from the coordinated ligand to the Sm^{III} ions is less efficient than that of the Eu^{III} and Tb^{III} complexes.

The Dy^{III} emission in complex **10** is weak but clear emission peaks at 475, 573, and 652 nm are observed at 77 K (see Figure S3 in the Supporting Information). However, the luminescence

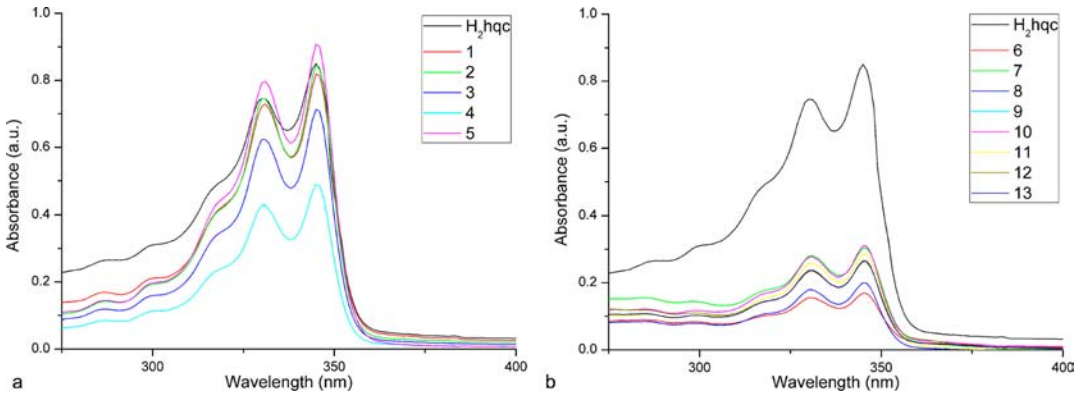

Figure 5. UV–vis absorption spectra of the ligand H_2hqc and complexes (a) **1–5** in DMF solution (2×10^{-5} M) and (b) **6–13** in DMF solution (2×10^{-5} M).

dx.doi.org/10.1021/ic301261g | Inorg. Chem. 2012, 51, 13128–13137

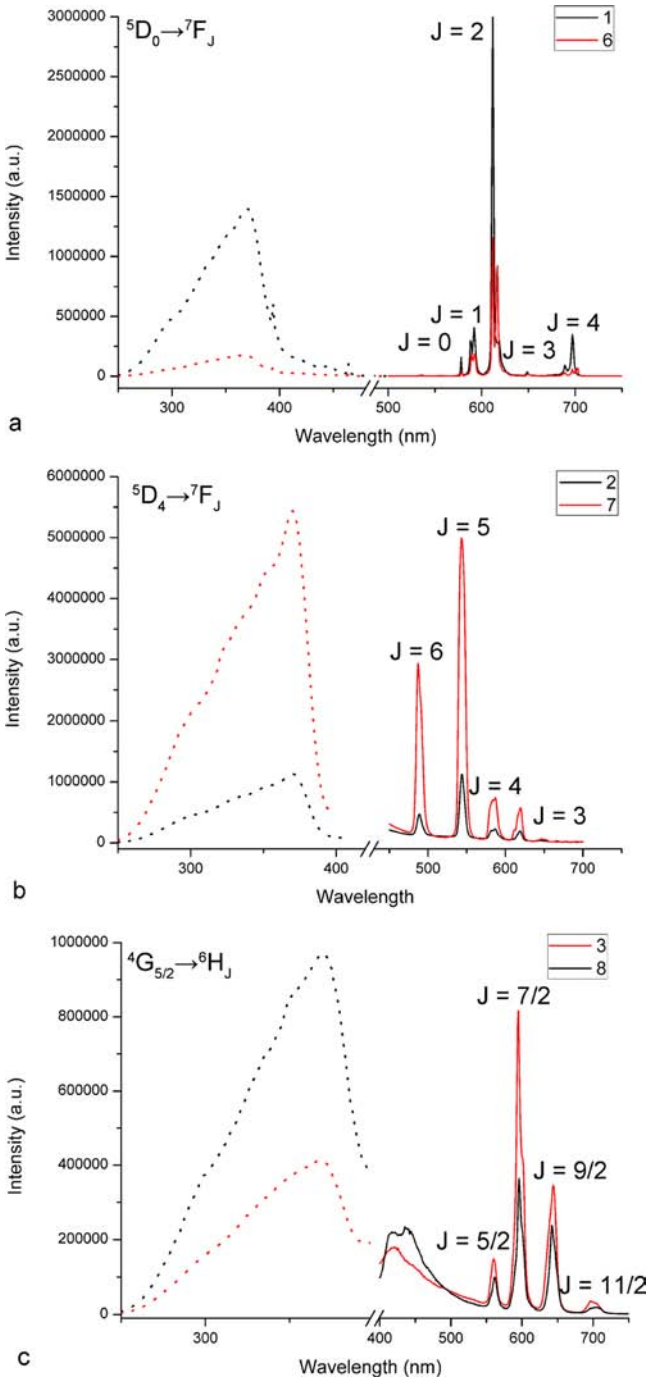

Figure 6. Room-temperature excitation (dotted line) and emission (solid line) spectra of the (a) Eu^{III} (b), Tb^{III}, and (c) Sm^{III} complexes in the solid state.

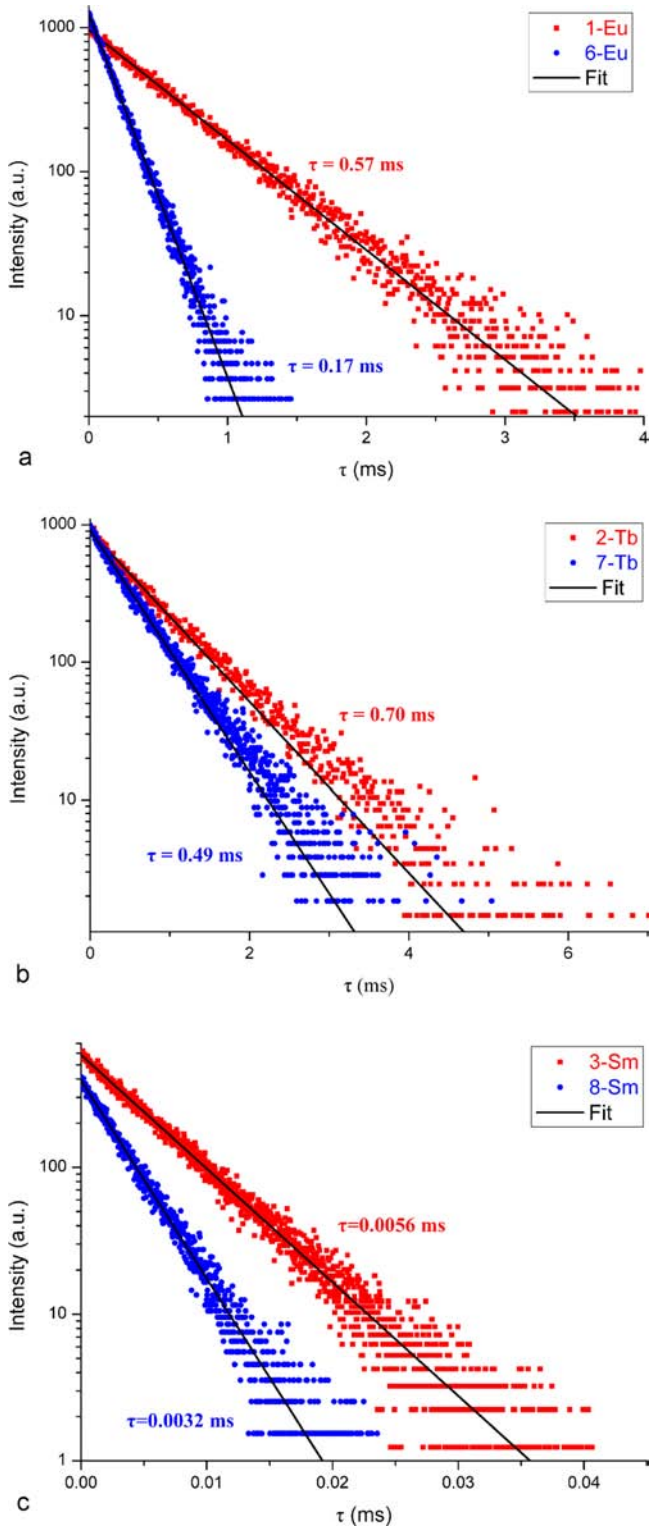

Figure 7. Luminescence decay curves for complexes (a) **1** and **6** for Eu^{III}, (b) **2** and **7** for Tb^{III}, and (c) **3** and **8** for Sm^{III}, each excited at 360 nm in the solid state at 77 K. The scattering points are experimental data, and the solid lines are the fitting results.

of Tm^{III} in complex **9** is too weak to be measured with our instrument setup.

Time-resolved fluorescence study was performed by monitoring the most intense emission bands at 77 and 298 K. The relevant data of luminescent lifetimes of complexes are listed in Table S4 in the Supporting Information. The decay curves of Eu^{III} ($^5D_0$), Tb^{III} ($^5D_4$), and Sm^{III} ($^4G_{5/2}$) complexes (**1**, **2**, **3**, **6**, **7**, and **8**) are well-produced by single-exponential functions at 77 K, as depicted in Figure 7, thus implying the existence of only one emissive Ln^{III} center. As shown in Figure 8, it is not surprising that the Eu^{III} and Sm^{III} complexes have somewhat shorter luminescence lifetimes than their corresponding Tb^{III} complexes since the Ln^{III} ions with smaller energy gaps are quenched more efficiently than those with larger energy gaps through nonradiative deactivation process.[18] On the other hand, the lifetimes of complexes **1**, **2**, and **3** are

dx.doi.org/10.1021/ic301261g | *Inorg. Chem.* 2012, 51, 13128−13137

complexes	1	6	2	7	3	8
τ (ms)	0.57	0.17	0.70	0.49	0.0056	0.0032

Figure 8. Images of complexes **1**–**3** and **6**–**8** under an UV lamp at 365 nm and the table of their lifetimes excited at 360 nm.

longer than their corresponding ox^{2-}-coordinated ones (**6**, **7**, and **8**) at 77 K. The above results are probably due to the different structures:

(a) $\pi\cdots\pi$ interactions of the conjugated ligands in complexes **1**–**3** may bring lumophores closer, which enables electronic interactions between the lumophores, thereby leading to the increase of emission lifetimes.[2a,19]

(b) The decreased coordinated water molecules in the first coordination sphere of Ln^{III} center for complexes **1**–**3** virtually decrease the nonradiative decay associated with vibrational coupling of excited states of Ln^{III} ions and OH oscillators, thus increasing the emission lifetimes.[20]

NIR LUMINESCENT PROPERTIES OF ND- AND YB-CENTERED COMPLEXES

Luminescence spectra of Nd^{III} and Yb^{III} complexes in solid state upon excitation at 397 nm display typical narrow band emissions in the NIR region at room temperature. For complexes **4** and **11**, the emission spectra (Figure 9a) consist of three bands at 888, 1055, and 1329 nm for **4** and 892, 1059, and 1326 nm for **11**, which are attributed to the $^4F_{3/2} \rightarrow {}^4I_{9/2}$, $^4F_{3/2} \rightarrow {}^4I_{11/2}$, and $^4F_{3/2} \rightarrow {}^4I_{13/2}$ transitions of Nd^{III} ions, respectively. For complex **12**, the emission spectrum contains one weak band at ~997 nm corresponding to the $^2F_{5/2} \rightarrow {}^2F_{7/2}$ transition of Yb^{III} ion (Figure 9b). This band splits slightly into three components, where the strongest is centered at 997 nm and the weaker two at 979 and 1011 nm. The luminescence lifetimes of these complexes are smaller than their corresponding Eu^{III}, Tb^{III}, and Sm^{III} complexes (see Table S4 in the Supporting Information), since the nonradiative deactivation process plays an accentuated quenching effect in NIR-emitting lanthanide ions, in comparison with the visible emitting lanthanide ions.

INTRAMOLECULAR ENERGY TRANSFER BETWEEN LIGANDS AND LN IONS

To investigate the energy transfer mechanism of complexes $[Ln(Hhqc)_3(H_2O)]_n \cdot 3nH_2O$, it is desirable to determine the energy levels of the relevant singlet and triplet excited states of the ligand H_2hqc. The singlet energy level of H_2hqc is calculated by referring to the upper wavelength of UV–vis absorption spectrum of the corresponding Gd^{III} complex (Figure 5).[21] The relevant value of the $^1\pi\pi^*$ for H_2hqc is 27 778 cm^{-1} (360 nm), which is more or less the same as the calculated one, based on time-dependent density functional theory (TD-DFT) calculation using Gaussian 03. The triplet energy level of the ligand is estimated by reference to the lower wavelength emission edge of the phosphorescence spectrum of the Gd^{III} complex at 77 K, in which the energy transfer does not occur for its higher energy than the sensitizing levels of the ligand.[22] Analysis of the phosphorescence emission, as illustrated in Figure S4 in the Supporting Information, shows

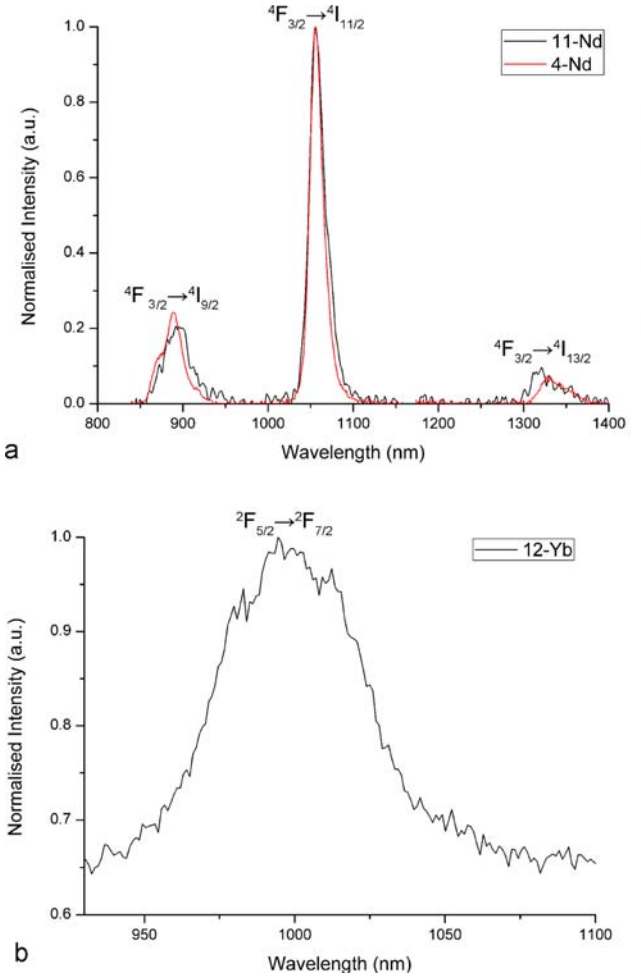

Figure 9. Room-temperature emission spectra of (a) the Nd^{III} complex and (b) the Yb^{III} complex, each in the solid state.

that the value of the $^3\pi\pi^*$ for H_2hqc is 21 367 cm^{-1} (468 nm), which is comparable to 21 746 cm^{-1} calculated by TD-DFT calculation. Thus, the energy gap of the singlet (27 778 cm^{-1}) and the triplet state (21 367 cm^{-1}) for H_2hqc is 6411 cm^{-1}, being larger than 5000 cm^{-1} and indicating that the intersystem crossing progress becomes effective according to Reinhoudt's empirical rule.[23] On the other hand, the triplet energy level of the H_2hqc ligand lies above the resonant level of Eu^{III} (17 267 cm^{-1}), Tb^{III} (20 500 cm^{-1}), and Sm^{III} (17 900 cm^{-1}) ions, thus allowing an efficient ligand-to-metal energy transfer.[24] By contrast, the resonant level of Tb^{III} in complex **2** at 20 500 cm^{-1} is found to be close to the triplet state of the H_2hqc ligand, which can lead to the thermally assisted back-energy transfer from the Tb^{III} ion.[25] Therefore, it supports the observation of lower quantum yield for Tb^{III} complex (0.06%) in contrast with its corresponding Eu^{III} and Sm^{III} complexes (17.35% and 0.16%, respectively) at room temperature. The pertinent data of quantum yield are listed in Table S4 in the Supporting Information.

To further investigate the energy transfer process between the ligands H_2hqc and H_2ox in complexes $[Ln(Hhqc)(ox)(H_2O)_2]_n$, the triplet energy level of H_2ox is estimated by phosphorescence of $[H_2N(CH_3)_2][Gd(ox)_2(H_2O)] \cdot 3H_2O$[26] at 77 K as shown in Figure 10c, and the singlet energy level of H_2ox is 38 462 cm^{-1}, according to the literature. The above experimental data, together with the excited energy level of

dx.doi.org/10.1021/ic301261g | Inorg. Chem. 2012, 51, 13128–13137

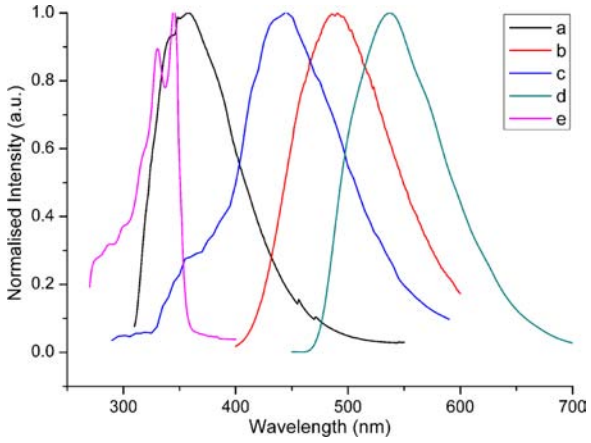

Figure 10. (a) Emission spectrum of H_2ox at room temperature excited at 298 nm. (b) Emission spectrum of H_2hqc at room temperature excited at 360 nm. (c) Phosphorescence spectrum of $[H_2N(CH_3)_2][Gd(ox)_2(H_2O)]\cdot 3H_2O$ at 77 K excited upon 290 nm. (d) Phosphorescence spectrum of $[Gd(Hhqc)_3(H_2O)]_n\cdot 3nH_2O$ at 77 K excited upon 290 nm. (e) UV−vis absorption spectrum of H_2hqc at room temperature.

H_2hqc, shed some light on the energy transfer process between ligands, since the singlet and triplet energy levels of H_2hqc are slightly lower than those of H_2ox. The presence of energy transfer involving the H_2hqc and H_2ox excited states is well-supported by the overlaps of the absorption spectra, room-temperature emission spectra, and phosphorescence spectra of these two ligands, as depicted in Figure 10. The overlap between the room-temperature emission of H_2ox and the absorption spectrum of H_2hqc allows for the energy transfer from the singlet state of H_2ox to the singlet state of H_2hqc. Meanwhile, the appearance of the overlap between the room-temperature emission spectrum of H_2ox and the phosphorescence spectrum of $[H_2N(CH_3)_2][Gd(ox)_2(H_2O)]\cdot 3H_2O$, as well as $[Gd(Hhqc)_3(H_2O)]_n\cdot 3nH_2O$ indicates the singlet state of H_2ox can also transfer energy to its own triplet level or to the triplet level of H_2hqc. The singlet state of H_2hqc can transfer the energy to the triplet state of H_2ox or its own triplet state provided by the overlap between the room-temperature emission of H_2hqc and the phosphorescence spectrum of H_2ox or H_2hqc. The triplet state of the ligand H_2ox can also transfer energy to the emission level of center Ln^{III} ions directly or through the triplet state of H_2hqc in light of the overlap of the phosphorescence spectra between $[Gd(Hhqc)_3(H_2O)]_n\cdot 3nH_2O$ and $[H_2N(CH_3)_2][Gd(ox)_2(H_2O)]\cdot 3H_2O$.

CONCLUSIONS

In summary, 13 novel lanthanide metal−organic coordination polymers with two types of compositions $[Ln(Hhqc)_3(H_2O)]_n\cdot 3nH_2O$ and $[Ln(Hhqc)(ox)(H_2O)_2]_n$ have been successfully synthesized, structurally characterized, and optically studied. Complexes **1**−**13** exhibit two-dimensional (2D) layer structures constructed by $Ln_2(CO_2)_4$ paddle-wheel units or Ln-ox infinite chains, respectively, cross-linked alternatively by bridging $Hhqc^-$ ligands. Upon UV excitation at room temperature, the ligand sensitizes the luminescence of the Ln^{III} ions emitting in the visible region for Eu^{III}, Tb^{III}, and Sm^{III} complexes as well as in the near-infrared (NIR) region for Nd^{III} and Yb^{III} complexes. Furthermore, the Tb^{III} complexes **2** and **7** exhibit bright green luminescence in solid state and possess longer excited-state lifetimes than the other complexes. Moreover, the increased π-rich ligands and decreased coordinated water molecules enhance the luminescence lifetimes obviously. The energy level of the triplet state of the ligand determined from the phosphorescence at 77 K of the Gd^{III} complex is higher than the resonant level of Ln^{III} ions ,demonstrating the potential of H_2hqc as an efficient ultraviolet (UV) light sensitizer for lanthanide-based visible and NIR emissions.

ASSOCIATED CONTENT

Supporting Information

The selected bond length and angle parameters of complexes **1**−**13**, PXRD patterns and TGA diagram for complexes **2**−**5** and **7**−**13**, and other supplementary figures of optical data. This material is available free of charge via the Internet at http://pubs.acs.org.

AUTHOR INFORMATION

Corresponding Author

*Tel.: +86-591-83792460. Fax: +86-591-83794946. E-mails: hmc@fjirsm.ac.cn (M.-C.H.), fjiang@fjirsm.ac.cn (F.-L.J.).

Notes

The authors declare no competing financial interest.

ACKNOWLEDGMENTS

We are thankful for financial support from 973 Program (Nos. 2011CBA00507 and 2011CB932504), National Nature Science Foundation of China (Nos. 21131006 and 20971121), and Nature Science Foundation of Fujian Province.

REFERENCES

(1) (a) Bunzli, J. C. G. *Chem. Rev.* **2010**, *110*, 2729−2755. (b) Bunzli, J. C. G. *Metal Complexes in Tumor Diagnosis and as Anticancer Agents*; Sigel, A., Sigel, H., Eds.; Metal Ions in Biological Systems, Vol. *42*; 2004; pp 39−75. (c) Kobayashi, H.; Ogawa, M.; Alford, R.; Choyke, P. L.; Urano, Y. *Chem. Rev.* **2009**, *110*, 2620−2640. (d) Kido, J.; Okamoto, Y. *Chem. Rev.* **2002**, *102*, 2357−2368. (e) Zheng, X. L.; Liu, Y.; Pan, M.; Lue, X. Q.; Zhang, J. Y.; Zhao, C. Y.; Tong, Y. X.; Su, C. Y. *Angew. Chem., Int. Ed.* **2007**, *46*, 7399−7403.

(2) (a) Allendorf, M. D.; Bauer, C. A.; Bhakta, R. K.; Houk, R. J. T. *Chem. Soc. Rev.* **2009**, *38*, 1330−1352. (b) Binnemans, K. *Chem. Rev.* **2009**, *109*, 4283−4374. (c) Carlos, L. D.; Ferreira, R. A. S.; Bermudez, V. D.; Ribeiro, S. J. L. *Adv. Mater.* **2009**, *21*, 509−534. (d) Eliseeva, S. V.; Bunzli, J. C. G. *Chem. Soc. Rev.* **2010**, *39*, 189−227. (e) Bunzli, J. C. G.; Piguet, C. *Chem. Soc. Rev.* **2005**, *34*, 1048−1077.

(3) (a) Xiao, Y. Q.; Cui, Y. J.; Zheng, Q. A.; Xiang, S. C.; Qian, G. D.; Chen, B. L. *Chem. Commun.* **2010**, *46*, 5503−5505. (b) Liu, D. Y.; Tang, K. Z.; Liu, W. S.; Su, C. Y.; Yan, X. H.; Tan, M. Y.; Tang, Y. *Dalton Trans.* **2010**, *39*, 9763−9765. (c) Hammell, J.; Buttarazzi, L.; Huang, C. H.; Morrow, J. R. *Inorg. Chem.* **2011**, *50*, 4857−4867.

(4) (a) Amiot, C. L.; Xu, S. P.; Liang, S.; Pan, L. Y.; Zhao, J. X. J. *Sensors* **2008**, *8*, 3082−3105. (b) Boyer, J. C.; Manseau, M. P.; Murray, J. I.; van Veggel, F. C. J. M. *Langmuir* **2010**, *26*, 1157−1164. (c) Chen, Z. G.; Chen, H. L.; Hu, H.; Yu, M. X.; Li, F. Y.; Zhang, Q.; Zhou, Z. G.; Yi, T.; Huang, C. H. *J. Am. Chem. Soc.* **2008**, *130*, 3023−3029. (d) Gaidamauskas, E.; Parker, H.; Kashemirov, B. A.; Holder, A. A.; Saejueng, K.; McKenna, C. E.; Crans, D. C. *J. Inorg. Biochem.* **2009**, *103*, 1652−1657.

(5) (a) Moore, E. G.; Samuel, A. P. S.; Raymond, K. N. *Acc. Chem. Res.* **2009**, *42*, 542−552. (b) Leonard, J. P.; Gunnlaugsson, T. *J. Lumin.* **2005**, *15*, 585−595. (c) de Lill, D. T.; de Bettencourt-Dias, A.; Cahill, C. L. *Inorg. Chem.* **2007**, *46*, 3960−3965.

(6) (a) Freund, C.; Porzio, W.; Giovanella, U.; Vignali, F.; Pasini, M.; Destri, S.; Mech, A.; Di Pietro, S.; Di Bari, L.; Mineo, P. *Inorg. Chem.*

2011, *50*, 5417−5429. (b) Zucchi, G.; Murugesan, V.; Tondelier, D.; Aldakov, D.; Jeon, T.; Yang, F.; Thuery, P.; Ephritikhine, M.; Geffroy, B. *Inorg. Chem.* **2011**, *50*, 4851−4856. (c) Li, H. F.; Yan, P. F.; Chen, P.; Wang, Y.; Xu, H.; Li, G. M. *Dalton Trans.* **2012**, *41*, 900−907. (d) Miyata, K.; Ohba, T.; Kobayashi, A.; Kato, M.; Nakanishi, T.; Fushimi, K.; Hasegawa, Y. *ChemPlusChem* **2012**, *77*, 277−280.

(7) (a) Guo, C. L.; Zhuo, X.; Li, Y. Z.; Zheng, H. G. *Inorg. Chim. Acta* **2009**, *362*, 491−501. (b) Wang, Y.; Song, Y.; Pan, Z. R.; Shen, Y. Z.; Hu, Z.; Guo, Z. J.; Zheng, H. G. *Dalton Trans.* **2008**, 5588−5592. (c) Wang, P.; Ma, J. P.; Dong, Y. B.; Huang, R. Q. *J. Am. Chem. Soc.* **2007**, *129*, 10620−10621. (d) Daiguebonne, C.; Kerbellec, N.; Guillou, O.; Bunzli, J. C.; Gumy, F.; Catala, L.; Mallah, T.; Audebrand, N.; Gerault, Y.; Bernot, K.; Calvez, G. *Inorg. Chem.* **2008**, *47*, 3700−3708. (e) Marchal, C.; Filinchuk, Y.; Chen, X. Y.; Imbert, D.; Mazzanti, M. *Chem.—Eur. J.* **2009**, *15*, 5273−5288.

(8) Tang, C. W.; Vanslyke, S. A. *Appl. Phys. Lett.* **1987**, *51*, 913−915.

(9) Hollingshead, R. G. W., *Oxine and Its Derivatives*, Vol. *I*; Butterworths: London, 1954.

(10) Feng, R.; Jiang, F. L.; Wu, M. Y.; Chen, L.; Yan, C. F.; Hong, M. C. *Cryst. Growth Des.* **2010**, *10*, 2306−2313.

(11) Sheldrick, G. M. *SHELXS-97, Programs for X-ray Crystal Structure Solution*; University of Göttingen: Göttingen, Germany, 1997.

(12) (a) Zhuang, G. L.; Kong, X. J.; Long, L. S.; Huang, R. B.; Zheng, L. S. *CrystEngComm* **2010**, *12*, 2691−2694. (b) Lu, W. G.; Jiang, L.; Lu, T. B. *Cryst. Growth Des.* **2010**, *10*, 4310−4318. (c) Qin, C.; Song, X. Z.; Su, S. Q.; Dang, S.; Feng, J.; Song, S. Y.; Hao, Z. M.; Zhang, H. J. *Dalton Trans.* **2012**, *41*, 2399−2407.

(13) (a) Liu, L. L.; Ren, Z. G.; Zhu, L. W.; Wang, H. F.; Yan, W. Y.; Lang, J. P. *Cryst. Growth Des.* **2011**, *11*, 3479−3488. (b) Qin, C.; Wang, X. L.; Wang, E. B.; Su, Z. M. *Inorg. Chem.* **2005**, *44*, 7122−7129. (c) Chen, M. S.; Su, Z.; Chen, M.; Chen, S. S.; Li, Y. Z.; Sun, W. Y. *CrystEngComm* **2010**, *12*, 3267−3276.

(14) Miyata, K.; Nakagawa, T.; Kawakami, R.; Kita, Y.; Sugimoto, K.; Nakashima, T.; Harada, T.; Kawai, T.; Hasegawa, Y. *Chem.—Eur. J.* **2011**, *17*, 521−528.

(15) (a) Dai, J. W.; Tong, M. L. *CrystEngComm* **2012**, *14*, 2124−2131. (b) Wang, Z. M.; Zhu, W. H.; Gao, S. *Inorg. Chem.* **2007**, *46*, 1337−1342. (c) Han, Y. F.; Li, X. Y.; Li, L. Q.; Ma, C. L.; Shen, Z.; Song, Y.; You, X. Z. *Inorg. Chem.* **2010**, *49*, 10781−10787.

(16) Chen, X. Y.; Liu, G. K. *J. Solid State Chem.* **2005**, *178*, 419−428.

(17) (a) Ofelt, G. S. *J. Chem. Phys.* **1962**, *37*, 511. (b) Judd, B. R. *Phys. Rev.* **1962**, *127*, 750.

(18) (a) Eliseeva, S. V.; Pleshkov, D. N.; Lyssenko, K. A.; Lepnev, L. S.; Bunzli, J. C.; Kuzmina, N. P. *Inorg. Chem.* **2010**, *49*, 9300−9311. (b) de Bettencourt-Dias, A.; Barber, P. S.; Viswanathan, S.; de Lill, D. T.; Rollett, A.; Ling, G.; Altun, S. *Inorg. Chem.* **2010**, *49*, 8848−8861.

(19) Cornil, J.; dos Santos, D. A.; Crispin, X.; Silbey, R.; Bredas, J. L. *J. Am. Chem. Soc.* **1998**, *120*, 1289−1299.

(20) (a) Richardson, F. S. *Chem. Rev.* **1982**, *82*, 541−552. (b) Stein, G.; Wurzberg, E. *J. Chem. Phys.* **1975**, *62*, 208−213.

(21) Raj, D. B.; Francis, B.; Reddy, M. L.; Butorac, R. R.; Lynch, V. M.; Cowley, A. H. *Inorg. Chem.* **2010**, *49*, 9055−9063.

(22) Carnall, W. T.; Fields, P. R.; Rajnak, K. *J. Chem. Phys.* **1968**, *49*, 4443.

(23) Steemers, F. J.; Verboom, W.; Reinhoudt, D. N.; Vandertol, E. B.; Verhoeven, J. W. *J. Am. Chem. Soc.* **1995**, *117*, 9408−9414.

(24) (a) Carnall, W. T.; Fields, P. R.; Rajnak, K. *J. Chem. Phys.* **1968**, *49*, 4450. (b) Carnall, W. T.; Fields, P. R.; Rajnak, K. *J. Chem. Phys.* **1968**, *49*, 4447. (c) Carnall, W. T.; Fields, P. R.; Rajnak, K. *J. Chem. Phys.* **1968**, *49*, 4424. (d) Latva, M.; Takalo, H.; Mukkala, V.-M.; Matachescu, C.; Rodriguez-Ubis, J. C.; Kankare, J. *J. Lumin.* **1997**, *75*, 149−169.

(25) Yu, J. A. *J. Lumin.* **1998**, *78*, 265−270.

(26) Complex $[H_2N(CH_3)_2][Gd(ox)_2(H_2O)]\cdot 3H_2O$ was synthesized in order to get the information about the triplet state of H_2ox. The synthesis process was explicated in the Supporting Information. Crystal data for $[H_2N(CH_3)_2][Gd(ox)_2(H_2O)]\cdot 3H_2O$:$C_6H_{16}N_1O_{12}Gd_1$, M_r = 451.44, monoclinic, space group $P2_1/n$, a = 9.658(9) Å, b = 11.707(8) Å, c = 12.282(10) Å, β = 99.239(5)°, V = 1370.69(19) Å^3, Z = 4, T = 293(2) K, D_c = 2.163 g cm^{-3}, $F(000)$ = 856, Mo Kα radiation (λ = 0.71073 Å), R_{int} = 0.0207, 10288 reflections collected, 3151 unique, μ = 4.898 mm^{-1}, R_1 (wR_2) = 0.0232 (0.0476), and GoF = 1.154 for 2940 reflections with $I > 2\sigma(I)$.